Supporting Information: Redox Potential Prediction of Iron(II)/Iron(III) Complexes: A Density Functional Theory and Graph Neural Network Approach

Fakhrul H Bhuiyan,[†] Hassan Harb,[‡] Rajeev Surendran Assary,[‡] and Álvaro Vázquez Mayagoitia*,[†]

†*Computational Science Division, Argonne National Laboratory, Lemont, IL 60439, USA*

‡*Materials Science Division, Argonne National Laboratory, Lemont, IL 60439, USA*

E-mail: vama@alcf.anl.gov

Modified `xyz2mol_tm` Method

In this work, a modified version of the `xyz2mol_tm` method was used to convert iron complex structures from Cartesian coordinates to `RDKit Mol` objects. The original `xyz2mol_tm` only required the 3D Cartesian coordinates of a metal complex structure and overall charge of the complex to convert a metal complex to an `RDKit Mol` object. This conversion involved first creating an initial adjacency matrix based on the Cartesian coordinates, identifying the ligand fragments from this matrix, estimating the ligand charges via an extended Hückel calculation[1] and updating the ligand charges to create `Mol` objects for the ligands.[2] Finally, a series of processing steps that include assessment of haptic bonds, charge adjustments in specific chemical groups, and chemical sanitization yielded the sanitized `Mol` object for the metal complex.[2,3]

Here, we modified the `xyz2mol_tm` routines to replace the initial step in which lig-

and fragments were identified from an adjacency matrix calculated from the 3D Cartesian coordinates and atomic covalent radii. Instead of relying on atomic covalent radii, our modified version uses bond orders calculated at the GFN2-xTB level to create the initial adjacency matrix and identify ligand fragments.[4] Bond orders exceeding specified cutoff values were used to define atomic connectivity. A cutoff of 0.25 was applied for bonds involving the Fe center, while a higher cutoff of 0.4 was used for all other atom pairs. The computed bond orders at the GFN2-xTB level provide a more accurate representation of the adjacency matrix than approximations based on covalent radii. Additionally, the modification allows full utilization of the tmQM dataset which provides the bond orders and atomic valence indices of the metal complexes calculated at the GFN2-xTB level.

Next, we added one new post-SMILES-generation cleaning step to `xyz2mol_tm` to produce chemically meaningful SMILES for nitroso groups ($-$NO) in metal complexes. This cleaning step is similar to the existing post-SMILES-generation cleaning steps for sulfonate group ($-SO_3^-$) and nitro group ($-NO_2$) in `xyz2mol_tm`. Finally, `xyz2mol_tm` was updated to produce the SMILES string along with the sanitized `Mol` object.

Collecting Desolvated Geometries for GNN Training Dataset

The first and the primary training dataset (GNN-Redox$_{1450}^{desolv-geo}$) used in this work was generated by collecting desolvated iron complexes obtained after removing all explicit solvent water molecules from the optimized, microsolvated structures used in the redox potential calculations. These desolvated structures differ from the structures in the tmQM dataset since the tmQM structures were initially obtained from the Cambridge Structural Database which contains experimentally determined crystal structures. These initial structures were then fully optimized in the gas phase with the extended tight-binding xTB method before being stored in the tmQM dataset.[4,5] As such, the tmQM structures may not fully represent the structures in solution, as the immediate coordination environment around the central metal ion can change in solution in the presence of water molecules. Compared to the

tmQM structures, the desolvated structures are better representations of the complexes and the metal ion coordination environment in a solution.

However, desolvated structures where the metal ion coordination environment deviate significantly from the tmQM structures can create a misleading representation of the complex in solution, as the solvent water molecules responsible for the change in the metal coordination environment are not present in the desolvated structures. Thus, the desolvated structures were filtered out if they deviated significantly from the original tmQM structures. Desolvated structures were discarded if any atom in the complex directly bonded to the iron center (i.e., first-shell neighbors) deviated by more than 0.7 Å from the atom's original position in the tmQM structure. This 0.7 Å cutoff value was selected to exclude highly dissimilar structures while maximizing structure retention. This comparison ensured structural consistency with the tmQM dataset and preserved the integrity of the ligand chemistry and coordination environments used in the training dataset.

Finally, the collected desolvated structures were converted from Cartesian coordinates to `RDKit Mol` objects using our modified `xyz2mol_tm` method. During the conversion from Cartesian coordinates to `Mol` objects, we automatically discarded a handful of complexes that could not be transformed into chemically valid `Mol` objects by our modified `xyz2mol_tm` method because of ambiguous bonding patterns or failed ligand-charge assignments. Additional quality checks were performed on the remaining structures. Specifically, complexes were discarded if the iron ion had more than eight direct neighbors. Further, complexes that did not contain the same number of ligands as their corresponding structures in the tmQM were discarded. After all filtering steps, a total of 1,450 iron complexes remained. These curated desolvated structures form what we refer to as the GNN-Redox$_{1450}^{desolv-geo}$ dataset, which was used for GNN model training and evaluation.

Model Hyperparameters

Graph Convolutional Network (GCN):

- `hidden_dim` = Hidden dimension size for all layers = 512
- `num_conv_layers` = Number of graph convolutional layers = 3
- `num_fc_layers` = Number of fully connected layers = 5
- `dropout` = Dropout probability for regularization = 0.1
- `norm_type` = Normalization type applied after each layer = layer
- `normalize_adj` = Whether to normalize adjacency matrix = True
- `self_msg` = Self-message aggregation strategy = add
- `batch_size` = Training batch size = 128
- `max_lr` = Maximum learning rate for scheduler = 1×10^{-3}
- `epochs` = Maximum training epochs = 200

Graph Attention Network (GAT):

- `hidden_dim` = Hidden dimension size for all layers = 512
- `num_heads` = Number of attention heads per layer = 3
- `num_conv_layers` = Number of graph attention layers = 3
- `num_fc_layers` = Number of fully connected layers = 5
- `dropout` = Dropout probability for regularization = 0.1
- `norm_type` = Normalization type applied after each layer = layer
- `add_residual` = Whether to use residual connections = True
- `batch_size` = Training batch size = 64
- `max_lr` = Maximum learning rate for scheduler = 1×10^{-3}
- `epochs` = Maximum training epochs = 200

DimeNet++:

- `hidden_channels` = Hidden embedding dimension = 128
- `num_blocks` = Number of interaction blocks = 4
- `int_emb_size` = Interaction embedding size = 64
- `basis_emb_size` = Basis function embedding size = 8

- `out_emb_channels` = Output embedding channels = 256
- `num_spherical` = Number of spherical harmonics = 7
- `num_radial` = Number of radial basis functions = 6
- `cutoff` = Interaction cutoff distance (Å) = 5.0
- `envelope_exponent` = Envelope function exponent = 5
- `num_before_skip` = Layers before skip connection = 1
- `num_after_skip` = Layers after skip connection = 2
- `num_output_layers` = Number of output layers = 3
- `batch_size` = Training batch size = 128
- `max_lr` = Maximum learning rate for scheduler = 1×10^{-3}
- `epochs` = Maximum training epochs = 400

SchNet:

- `hidden_channels` = Hidden embedding dimension = 128
- `num_filters` = Number of convolutional filters = 128
- `num_interactions` = Number of interaction blocks = 6
- `num_gaussians` = Number of Gaussian basis functions = 50
- `cutoff` = Interaction cutoff distance (Å) = 8.0
- `readout` = Global pooling aggregation method = add
- `dipole` = Whether to predict dipole moments = False
- `batch_size` = Training batch size = 128
- `max_lr` = Maximum learning rate for scheduler = 1×10^{-3}
- `epochs` = Maximum training epochs = 2000

Common Training Parameters: All models used Adam optimizer with cosine annealing learning rate scheduler, starting from an initial learning rate of 1×10^{-4}, warming up to the maximum learning rate over 2 epochs. Early stopping with a patience of 100 epochs was applied for the SchNet model, while patience was set to 50 for all other models.

Exchange correlation and basis set comparison

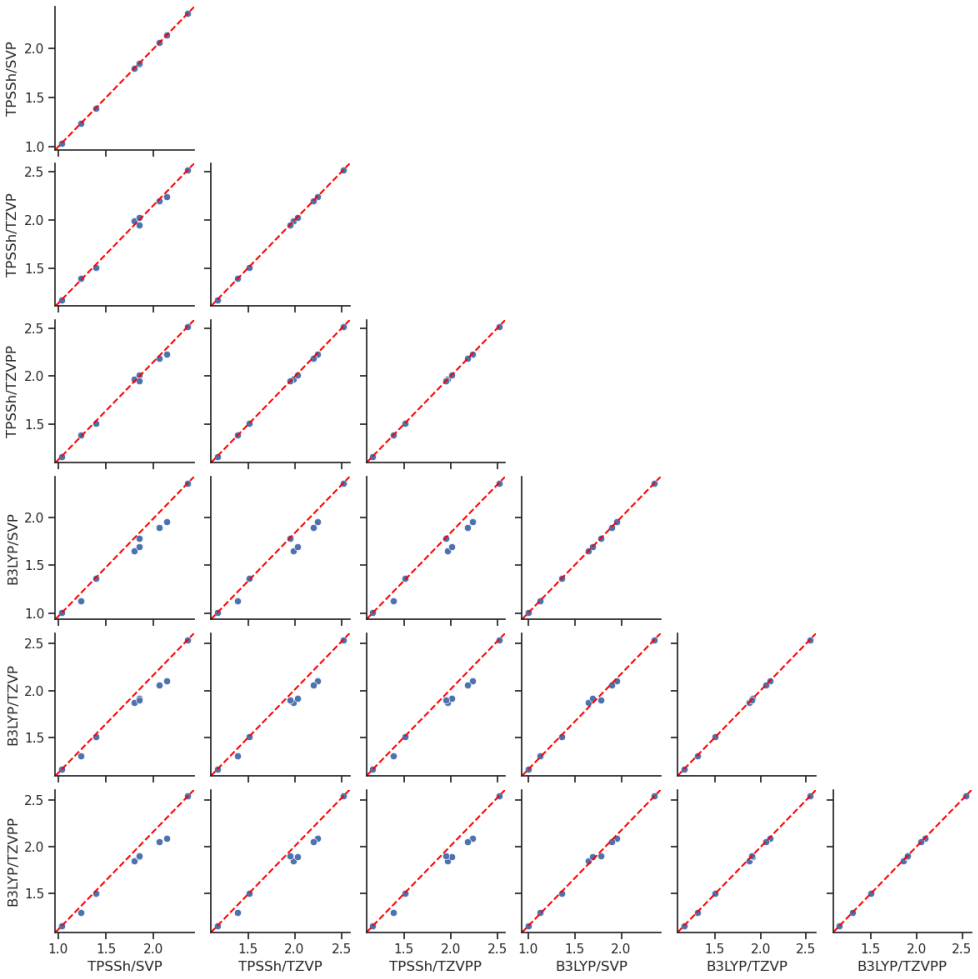

Figure S1: Comparison of redox potential (V) between TPSSh and B3LYP functional and SVP, TZVP and TZVPP basis set. For the tmQM Fe-complexes: XESNER, INAMAO, SESLUX, CPDOFE, REHZEK, CPFEFP, CPFEHQ, ACODUR and FURROZ.

Other Supporting Information

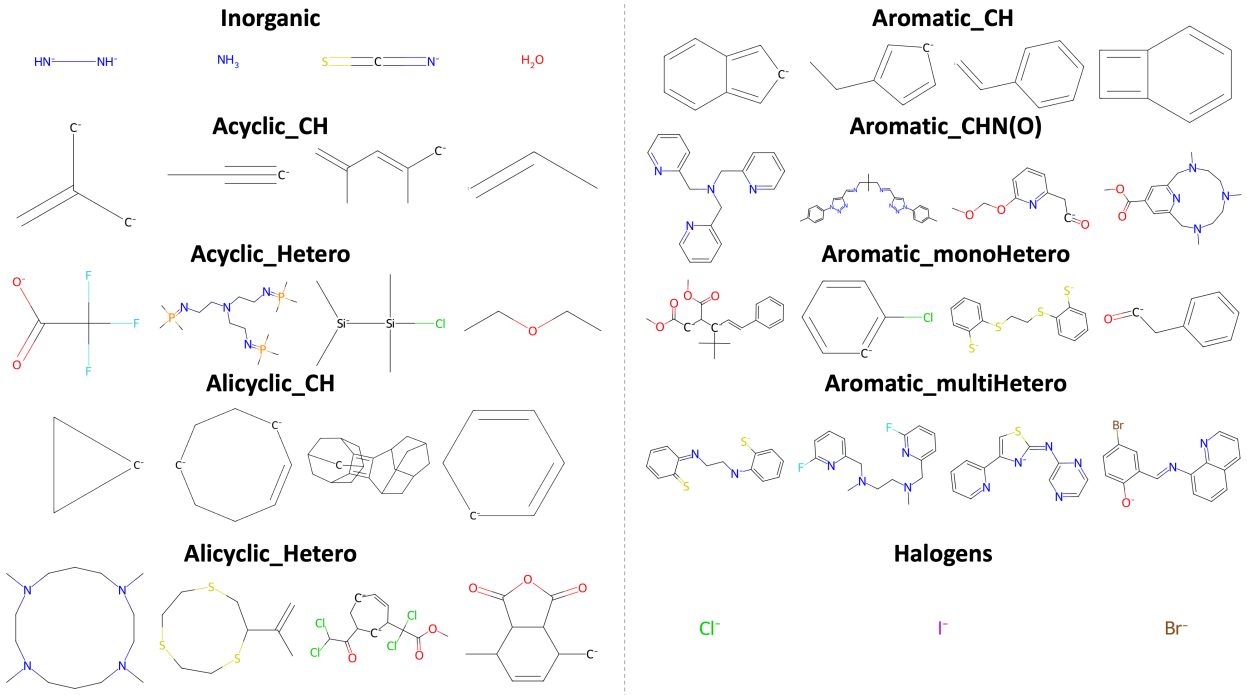

Figure S2: Randomly chosen example ligands from each of the 10 different classes distinguished in this study.

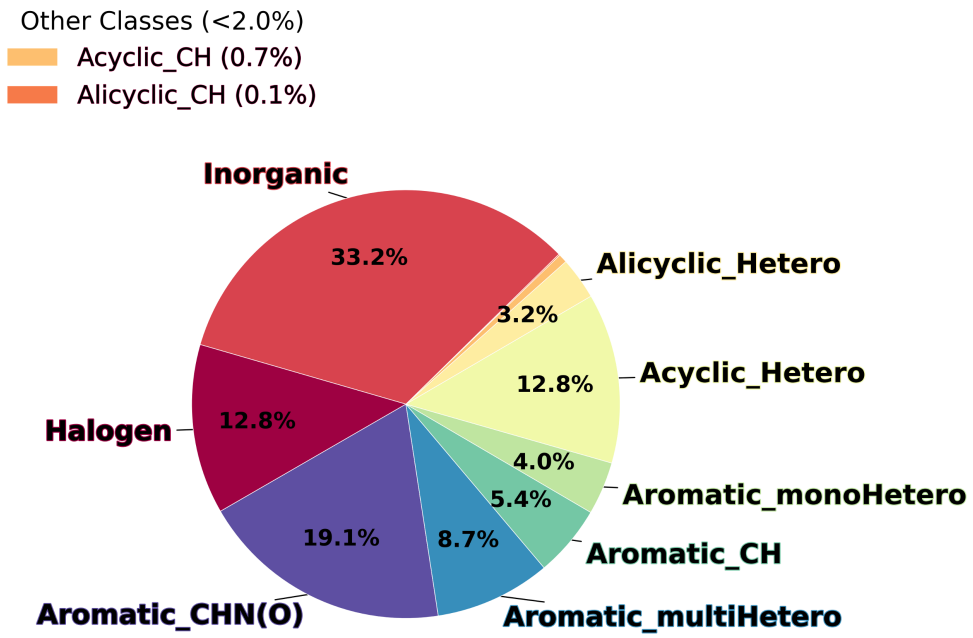

Figure S3: Ligand class distribution in the GNN-Redox$^{desolv-geo}_{1450}$ dataset that was used for GNN model training.

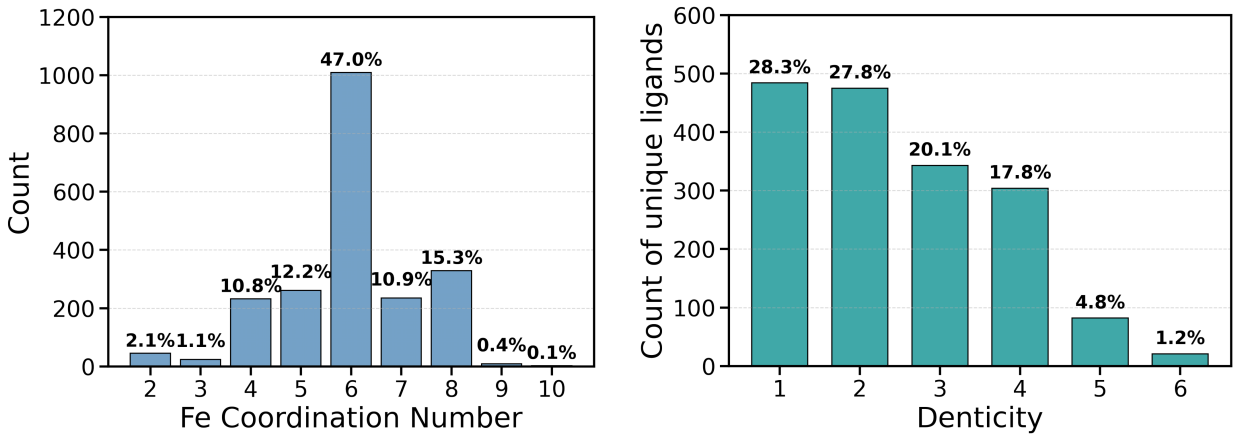

Figure S4: Distribution of (left panel) iron coordination number and (right panel) Ligand denticity in the Redox$_{2k}$ dataset.

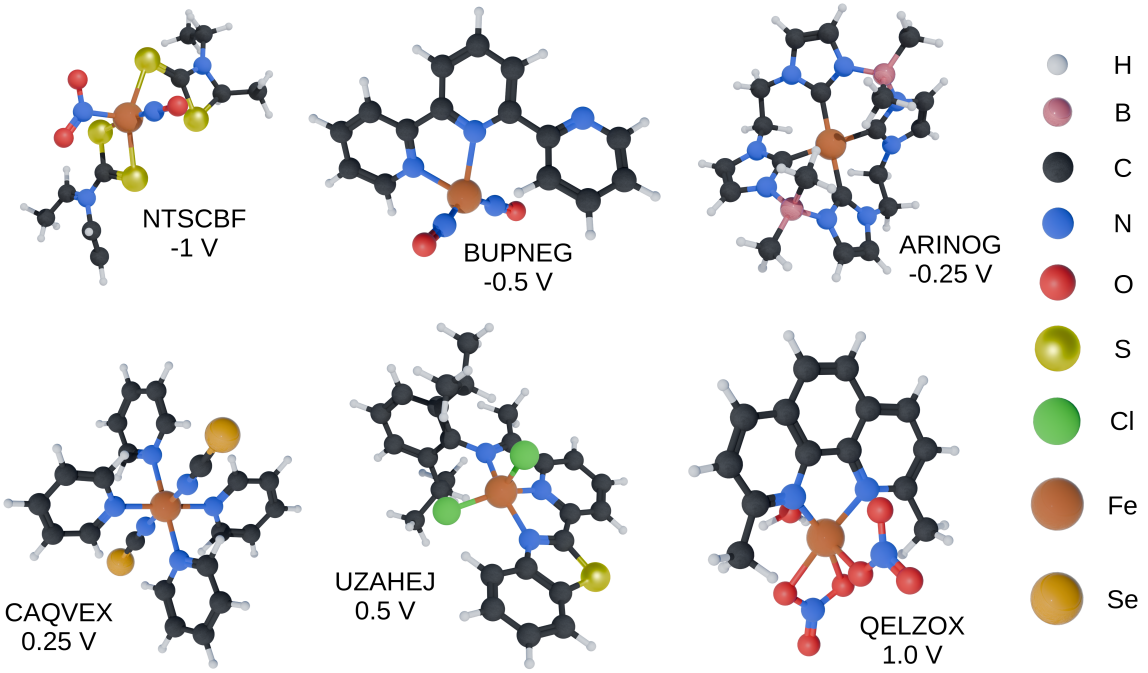

Figure S5: Randomly selected iron complexes from the Redox$_{2k}$ dataset, their CSD code-name, and calculated redox potential.

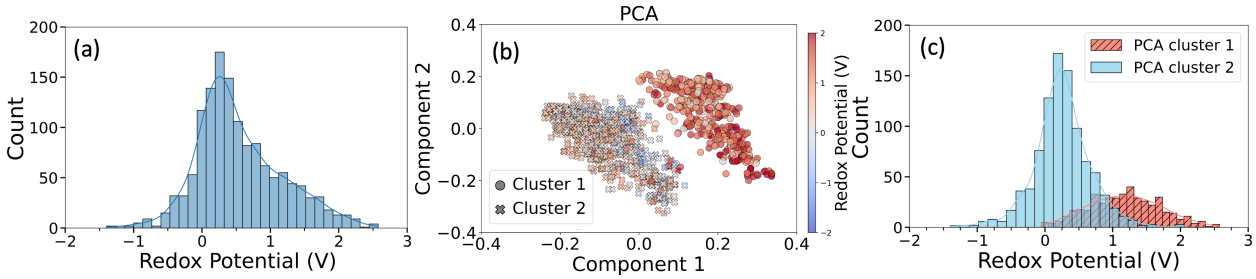

Figure S6: (a) Distribution of the redox potentials in the GNN-Redox$^{desolv-geo}_{1450}$ dataset. (b) The distribution of the iron complexes in the top two component space of the principal component analysis performed on the Morgan fingerprint of the complexes. The iron complexes diverged into two distinct clusters which were formally defined using k-means clustering algorithm, (c) Distribution of the redox potentials of the two clusters detected in the PCA space in (b).

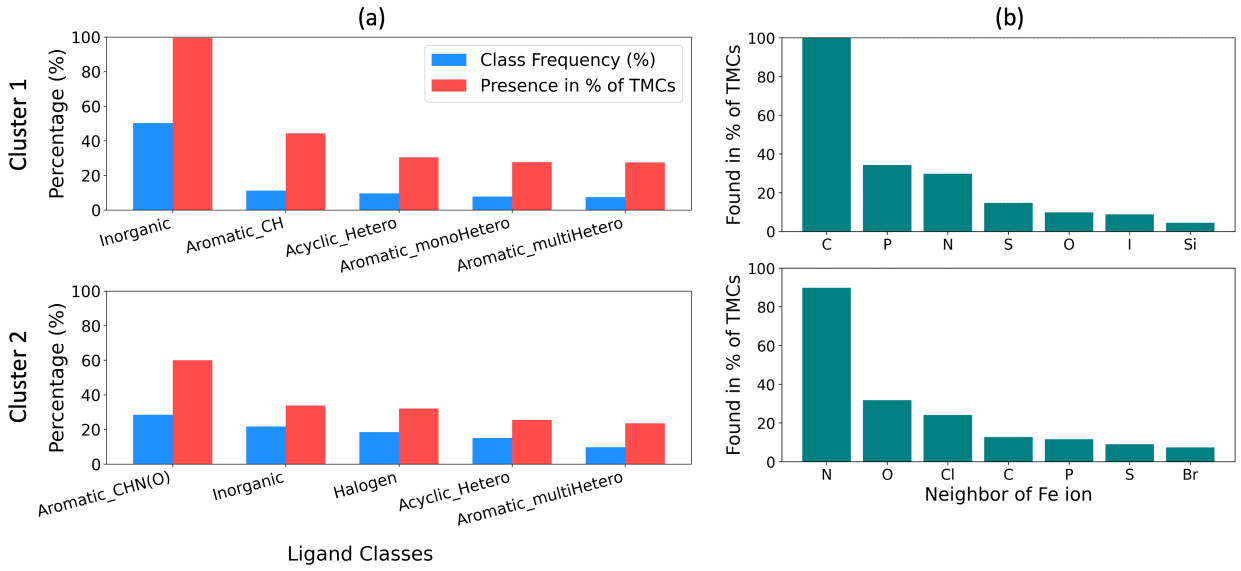

Figure S7: Analysis of the two clusters observed in the PCA space in Figure S6. (a) Analysis of the ligand classes, as defined in Figure 2, in the two clusters. The blue bars represent the frequency of ligand classes observed in all ligands of cluster 1 (top panel) and cluster 2 (bottom panel). Only the five most frequent ligand classes are shown. The red bars represent the percentage of iron complexes that contain a ligand from a specific class. (b) Analysis of the direct neighbors of the iron ion in the two clusters. The bars represent the percentage of iron complexes that contain a specific element as a neighbor.

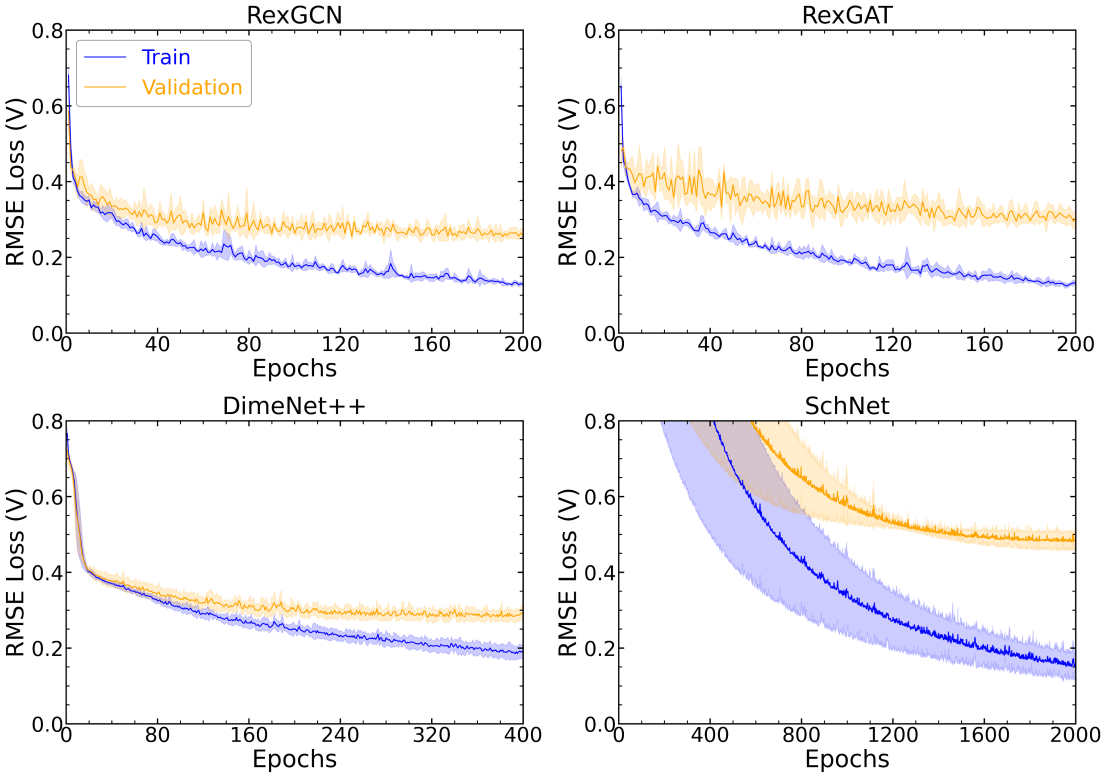

Figure S8: Train and validation RMSE loss of the RexGCN, RexGAT, DimeNet++, and SchNet models in cross validation (CV). Training was run for 200 epochs for the RexGCN and RexGAT models, 400 epochs for the DimeNet++ models, and 2,000 epochs for the SchNet models. CV was conducted with 3 folds for the SchNet model, and 5 folds for all other models. The solid lines represent the average of 5 CV folds (3 folds for SchNet) while the shaded region shows one standard deviation from the average.

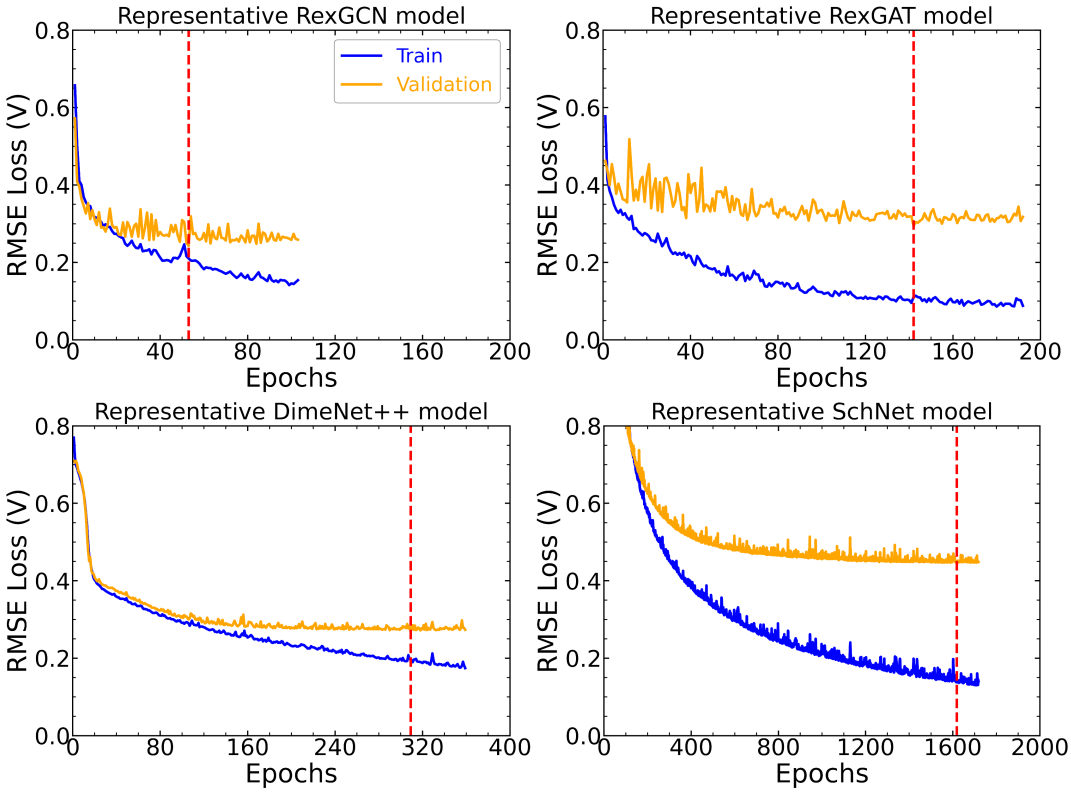

Figure S9: Train and validation RMSE loss of the representative RexGCN, RexGAT, DimeNet++, and SchNet models. Training was run for 200 epochs for the RexGCN and RexGAT models, 400 epochs for the DimeNet++ models, and 2,000 epochs for the SchNet models. The red dashed line in the inset marks the ignition of the early-stopping criteria and the best validation loss.

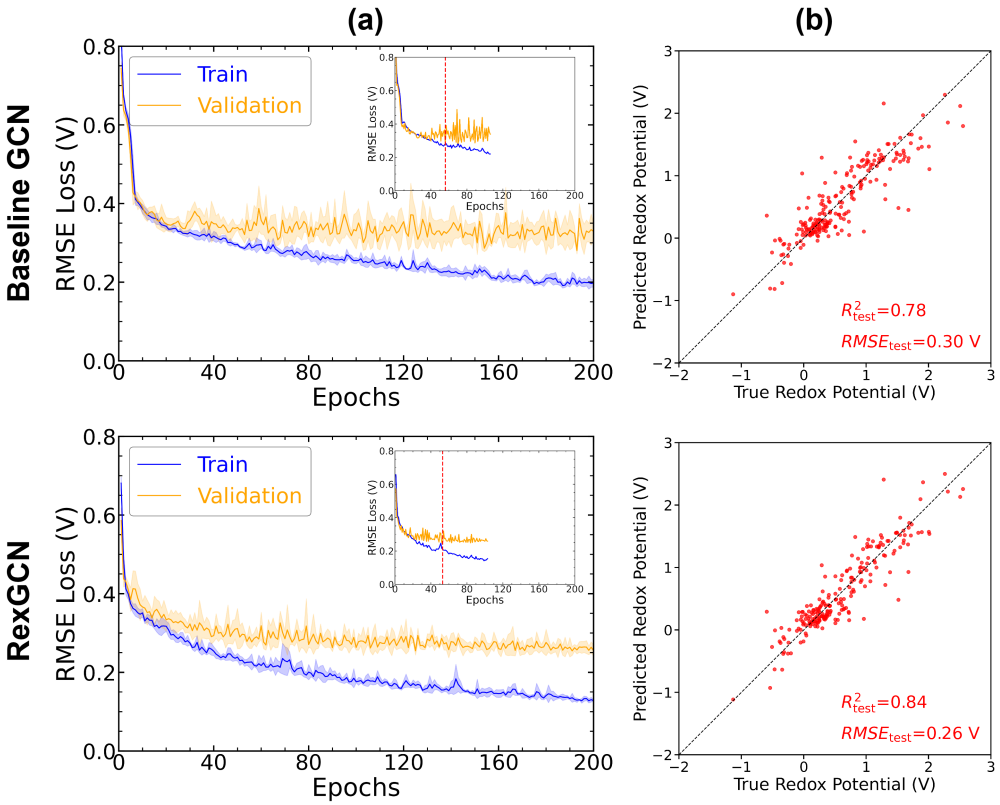

Figure S10: Performance comparison between the baseline GCN model with no edge features and our implementation of GCN model with edge features, i.e., RexGCN. (a) Train and validation RMSE loss of the baseline GCN (top) and RexGCN (bottom) models in the 5-fold CV. The solid lines represent the average of the 5 folds while the shaded region shows one standard deviation from the average. Inset shows the loss curve of the representative model. The red dashed line in the inset marks the ignition of the early-stopping criteria and the best validation loss. (b) Parity plot for the baseline GCN (top) and RexGCN (bottom) models showing performance on the test set.

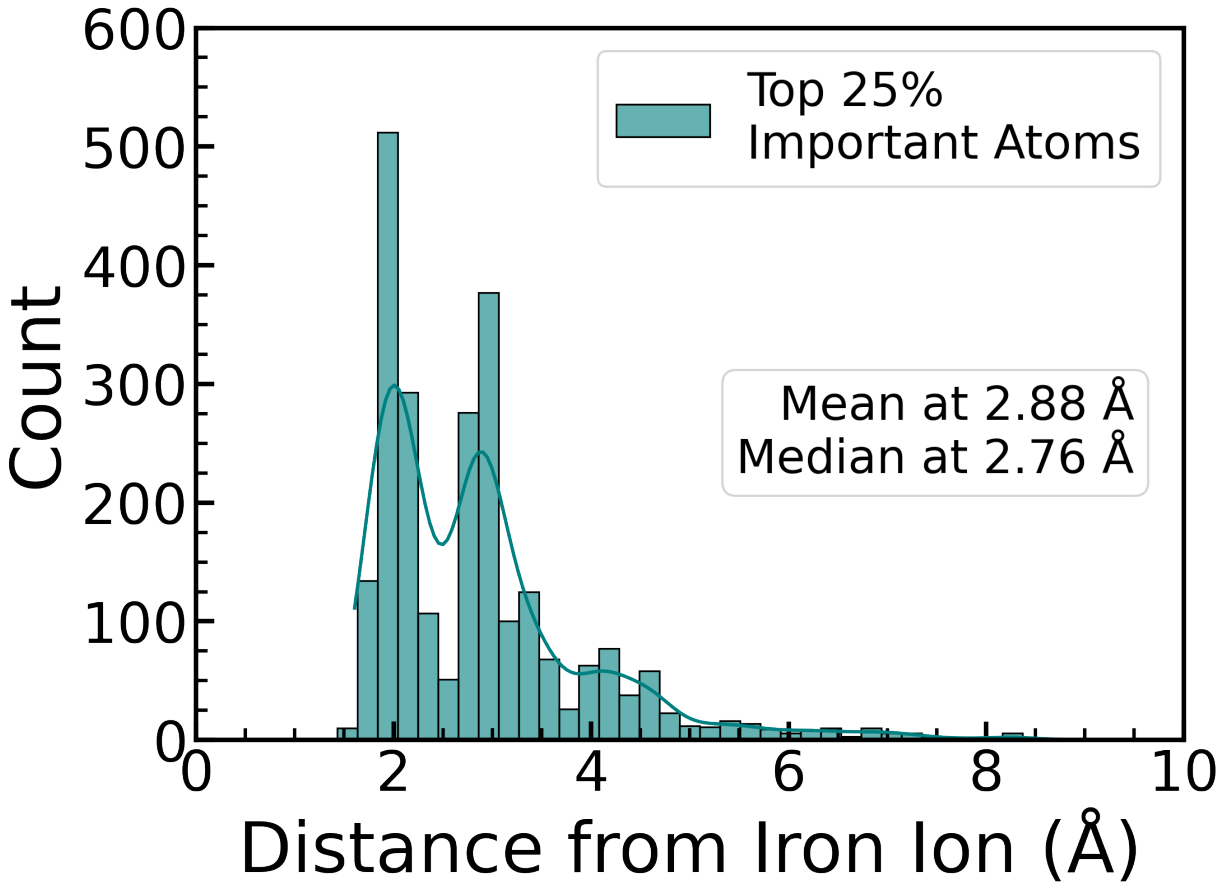

Figure S11: Distribution of distances between the central iron ion and the top 25% most important neighbor atoms, as determined by the feature attribution analysis, in all iron complexes in test set.

References

(1) Hoffmann, R. An extended Hückel theory. I. hydrocarbons. *The Journal of Chemical Physics* **1963**, *39*, 1397–1412.

(2) Rasmussen, M. H.; Strandgaard, M.; Seumer, J.; Hemmingsen, L. K.; Frei, A.; Balcells, D.; Jensen, J. H. SMILES all around: structure to SMILES conversion for transition metal complexes. *Journal of Cheminformatics* **2025**, *17*, 1–13.

(3) Kim, Y.; Kim, W. Y. Universal structure conversion method for organic molecules: from atomic connectivity to three-dimensional geometry. *Bulletin of the Korean Chemical Society* **2015**, *36*, 1769–1777.

(4) Bannwarth, C.; Ehlert, S.; Grimme, S. GFN2-xTB—An Accurate and Broadly Parametrized Self-Consistent Tight-Binding Quantum Chemical Method with Multipole Electrostatics and Density- Dependent Dispersion Contributions. *J. Chem. Theory Comput.* **2019**, *15*, 1652–1671.

(5) Balcells, D.; Skjelstad, B. B. tmQM dataset—quantum geometries and properties of 86k transition metal complexes. *Journal of chemical information and modeling* **2020**, *60*, 6135–6146.